Neuron, Volume *105*

Supplemental Information

Cortical Output Is Gated by Horizontally Projecting Neurons in the Deep Layers

Robert Egger, Rajeevan T. Narayanan, Jason M. Guest, Arco Bast, Daniel Udvary, Luis F. Messore, Suman Das, Christiaan P.J. de Kock, and Marcel Oberlaender

Supplemental Videos

Video S1 (related to Figure 3): Examples of *in silico* wRF mappings in L5PT model.

Supplemental Figures

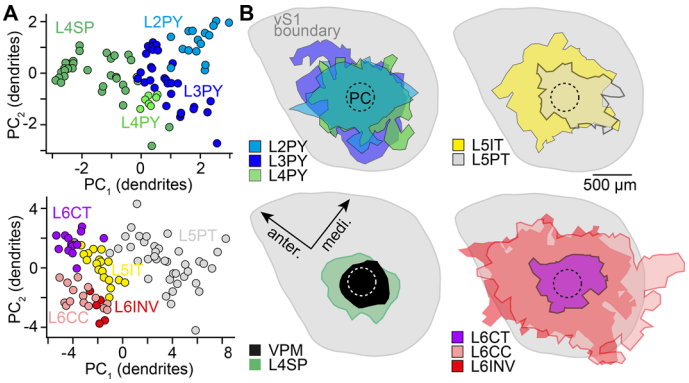

Figure S1 (related to Figure 1): Classification of *in vivo* labeled neurons into axo-dendritic cell types. A) Principal components ($PC_{1/2}$) of dendritic features (see (Narayanan et al., 2015)) that discriminate between axo-dendritic cell types in the upper and deep layers, respectively. **B)** Horizontal axon extent for each axo-dendritic cell type (i.e., the respective somata are located within the principal barrel column representing the C2 whisker (PC)).

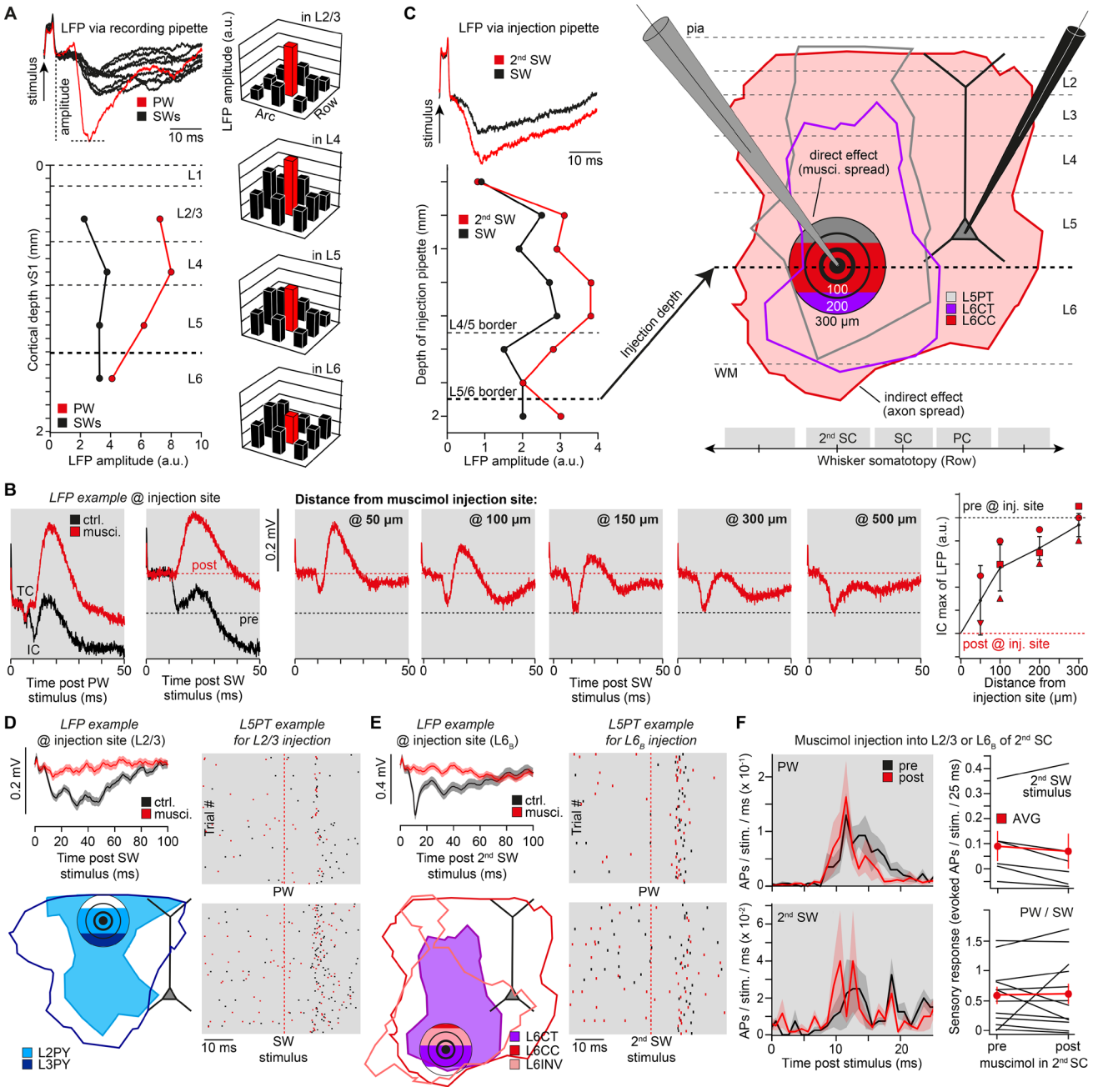

Figure S2 (related to Figure 5): LFP guided *in vivo* pharmacology. A) Left panel: LFP recordings via search pipette at 400 µm depth in vS1. LFP amplitudes in response to deflections of the PW and its eight SWs were quantified. Right panel: LFP wRF reveals the PW at the recording site (Lee et al., 2015) (here: C2). LFP wRF measurements were repeated at different cortical depths of vS1. Using the depth of layer borders (Meyer et al., 2013), the characteristic laminar profiles of LFP responses to PW (and SW) stimuli were used to identify the border between layer 4 and 5 (i.e., ~100 µm below the LFP maximum). The target location at the layer 5/6 border was hence approximately 400-500 µm below the LFP maximum. **B)** Complete deactivation of IC activity by muscimol injections was restricted to a volume of less than 100 µm in diameter. Injections had no direct pharmacological effect on neurons more distant than 300 µm from the injection site (i.e., no muscimol spread to layer 4 or the adjacent SCs). **C)** Example experiment

that illustrates how the LFP depth profile was used to locate the L5/6 border of the barrel column representing the manipulated 2nd SW (here: E2). The muscimol injection pipette was inserted rostral to vS1 at an angle that was approximately parallel to the midline (i.e., oblique to the vertical axis of vS1). E2 was identified as the manipulated 2nd SW based on the larger LFP amplitudes across the cortical depth when compared to those evoked by SW stimuli (shown here: E1). The target location (i.e., layer 5/6 border) was then determined by identifying the depth of maximal LFP amplitude and adding 500 µm (i.e., here injection at ~1,850 µm depth). Before and after muscimol injections, APs of L5PTs were recorded, whose respective PWs were separated by one whisker from the manipulated one (e.g. PW at the recording site is B2, the manipulated 2nd SW is D2, and the separating whisker is C2). Axonal extent from neurons located in the 2nd SC show that only L6CCs within the injection volume could directly impact L5PT responses at the recording site. **D)** Example LFPs before and after muscimol injections, recorded at the injection site around the border between layer 2 and 3. Corresponding AP responses in layer 5 evoked by the PW and manipulated whisker. Axonal extent from neurons located in the 2nd SC show that primarily L3PYs within the injection volume could directly impact L5PT responses at the recording site. **E)** Example LFPs before and after muscimol injections, recorded at the injection site in deep layer 6 (~1,800 µm underneath the pial surface). Corresponding AP responses in layer 5 evoked by the PW and manipulated whisker. Axonal extent from neurons located in the 2nd SC show that L6INVs within the injection volume could directly impact L5PT responses at the recording site. **F)** PW and 2nd SW evoked PSTHs across recorded L5PTs (n=6) before and after muscimol injections into layers 2/3 or deep layer 6 of the respective 2nd SC. Right panels: response per L5PT to stimulation of the 2nd SW and non-manipulated whiskers (i.e., PW and SW) before and after muscimol injections (mean ± SEM). Panels D-F are analogous to those shown for injections at the layer 5/6 border in **Figure 5**.

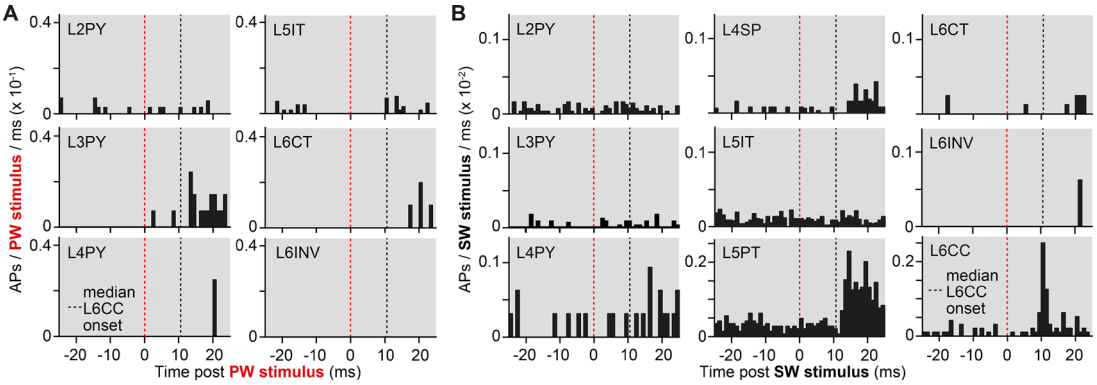

Figure S3 (related to Figure 7): Cell type-specific functional constrains for *in silico* experiments. **A)** PSTHs of PW evoked APs for morphologically classified neurons: L2PY (n=7), L3PY (n=7), L4PY (n=2), L5IT (n=13), L6CT (n=5) and L6INV (n=1), analogous to those shown in **Figure 7C** for L4SPs, L5PTs and L6CCs. **B)** PSTHs of SW evoked APs for all cell types (i.e., averaged across the eight SWs), representing the cells shown in panel A, **Figures 1** and **7C**.

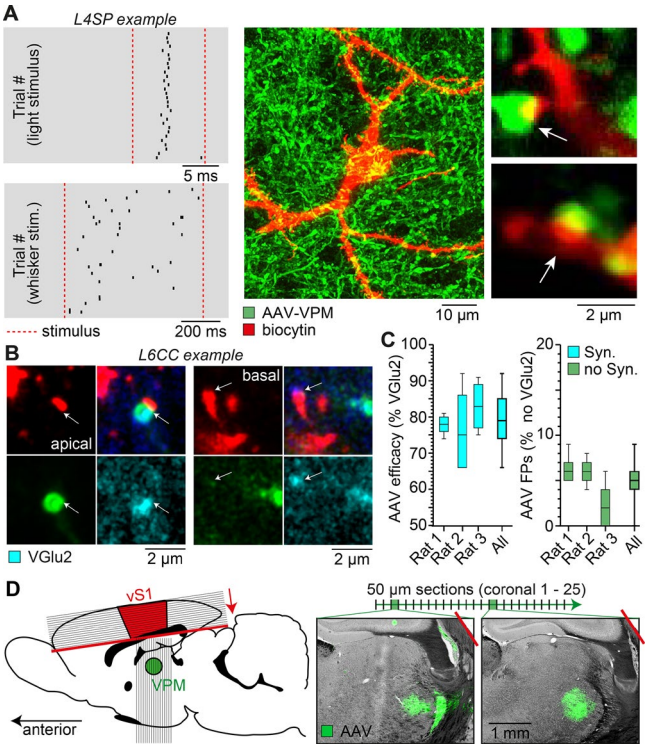

Figure S4 (related to Figure 8): Quantification of AAV injections. A) Example of cell-attached *in vivo* recording in layer 4 of AAV-injected brain. Ticks represent APs in response to a 10 ms flash of green light onto the cortical surface and a 700 ms airpuff onto the whiskers, respectively. Confocal images identify the recorded neuron as a L4SP. Putative TC synapses were identified as contacts between VPM boutons and dendritic spines. **B)** Super-resolution microscopy of the L6CC shown in **Figure 8**. Left panels show exemplary TC synapse along the apical dendrite (i.e., co-localized with VGlu2). Right panel shows exemplary TC synapse that was not labelled by the AVV injection into the VPM. **C)** Left panel: Fractions

of VGlu2-positive boutons (n=884) in layer 4 and at the layer 5/6 border of vS1 that were infected by AAV injections into the VPM (i.e., efficacy of the AAV is ~80%). Right panel: Fractions of the AAV-positive swellings (n=739) that were identified as TC boutons, but which did not co-express VGlu2 (i.e., false positive (FP) TC synapses). **D)** AAV injections sites for the L6CC shown in **Figure 8**. Cortex was cut into consecutive sections tangentially to vS1, the rest of the brain was cut coronally.

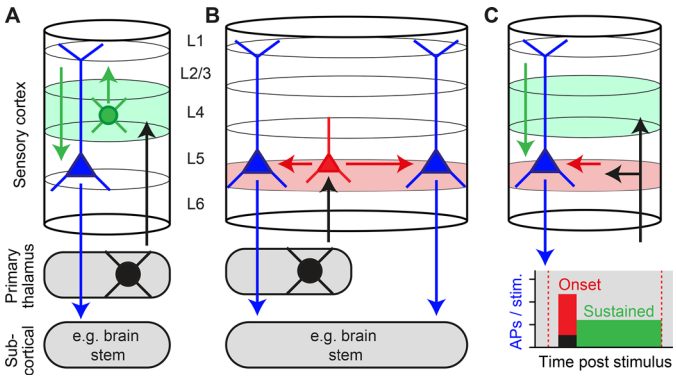

Figure S5 (related to Figure 8): Suggested concept of primary sensory cortex. Sensory-evoked TC input is relayed in parallel by two orthogonally organized thalamorecipient populations which give rise to complementary canonical pathways: vertical to layers 2/3 by L4SPs **(A)**, and horizontally to layers 5/6 by L6CCs **(B)**. The deep thalamorecipient pathway activates L5PTs, whereas signal flow in the upper layers terminates in layer 5. **C)** The complementary pathway theory hence provides a potential explanation for sustained AP responses in L5PTs that persist for the duration of the stimulus. We showed that one way to drive cortical output is by providing sufficiently strong and synchronous synaptic input to the proximal dendrites. However, synchrony decreases during recurrent excitation within local and long-range cortical circuits. Moreover, a substantial fraction of these recurrent and top-down inputs will impinge onto distal dendrites (e.g. within layer 1). It is hence unlikely that sustained responses in L5PTs originate from the same mechanism as the onset responses (see also (Rojas-Piloni et al., 2017)). We thus hypothesize that the L6CC gated onset responses are required to switch the apical dendrites into an active state, which allows L5PTs to transform temporally less synchronous and spatially more distributed synaptic inputs (e.g. from layers 2/3) into sustained patterns.

Supplemental Tables

Presynaptic cell type	Measurement (Reference)	Network model (L5PT population)	Network model (L5PT model)
L2PY	0.08 (Lefort et al., 2009)	0.07 ± 0.09*	0.13 ± 0.02
L3PY	0.12/0.55 (Lefort et al., 2009, Thomson et al., 2002)	0.15 ± 0.16*	0.34 ± 0.02
L4 (SP, PY)	0.08 (Lefort et al., 2009)	0.14 ± 0.15*	0.33 ± 0.04
L5IT	0.19 (Brown and Hestrin, 2009)	0.17 ± 0.13*	0.19 ± 0.05
L5PT	0.05-0.2 (Brown and Hestrin, 2009, Perin et al., 2011, Song et al., 2005)	0.23 ± 0.19*	0.24 ± 0.06
L6 (CC, INV, CT)	0.02 (Lefort et al., 2009)	0.13 ± 0.14*	0.15 ± 0.02
VPM	0.44 ± 0.17 (Constantinople and Bruno, 2013)	0.40 ± 0.12	0.39 ± 0.05
INH	0.22 (Thomson et al., 1996)	0.41 ± 0.14	0.26 ± 0.02

Table S1 (related to Figure 2). Cell type-specific connection probabilities. Comparison between predicted connection probabilities in vS1 network model and previously reported measurements from paired-recordings *in vitro* or *in vivo* (mean ± STD). The * denotes predicted connection probabilities between truncated morphologies in 300 µm thick thalamocortical/semi-coronal slices of the network model, because the respective empirical data was acquired in 300 µm thick acute brain slices *in vitro*.

Parameter	Soma	AIS / Myelin	Apical dendrite	Basal dendrites
C_m (μF/cm^2)	1.0	1.0 / 0.04	2.0	2.0
r_a (Ωcm)	100	100 / 100	100	100
g_{pas} ($1/r_m$)	0.326	0.256 / 0.4	0.882	0.631
Na_t	24300	880 / –	252	–
Na_p	49.9	14.6 / –	–	–
K_t	471	841 / –	–	–
K_p	0	7730 / –	–	–
SKv3.1	9830	9580 / –	112	–
SK E2	492	0.577 / –	34	–
Ca_{LVA}	46.2	85.8 / –	1040*	–
Ca_{HVA}	6.42	6.92 / –	45.2*	–
τ_{Ca} (ms)	770	507 / –	133	–
γ_{Ca} (1)	0.000616	0.0175 / –	0.0005	–
I_m	–	– / –	1.79	–
I_h	0.8	0.8 / –	$A+B\cdot\exp(C\cdot d/d_{max})$ **	2

Table S2 (related to Figure 3). Biophysical parameters of the L5PT model. These parameters were obtained using the multi-objective optimization algorithm described previously (Druckmann et al., 2007, Hay et al., 2011). Units for different ion channel densities are pS/μm^2. τ_{Ca} (ms) is the time constant of the calcium buffering model, and γ_{Ca} is a dimensionless parameter describing the calcium buffer affinity. g_{pas}: passive membrane conductance; Na_t: fast inactivating sodium current; Na_p: persistent sodium current; K_t: fast inactivating potassium current; K_p: slow inactivating potassium current; SKv3.1: fast non-inactivating potassium current; SK E2: calcium-activated potassium current; Ca_{LVA}: low voltage-activated calcium current; Ca_{HVA}: high voltage-activated calcium current; I_m: muscarinic potassium current; I_h: non-specific cation current. * Density in the calcium "hot zone" between 900-1100 μm from the soma. The density of low- and high-voltage activated calcium channels in the apical dendrite was set to 1% and 10% of that value, respectively, outside of the "hot zone". ** The density of I_h in the apical dendrite increases exponentially with distance d to the soma, with parameters A = -0.8696 pS/μm^2, B = 2.087pS/μm^2, C=3.6161, and d_{max} the distance of the apical dendrite top located the furthest from the soma. Voltage- and time-dependence of ion channels was modeled using the HH formalism. All corresponding parameters were taken from the literature and have been described in detail previously (Hay et al., 2011).

Feature	Mean ± STD	Model	Difference (STD)
Ca^{2+} AP peak	6.73 ± 2.54 mV	10.8 mV	1.6
Ca^{2+} AP width	37.43 ± 1.27 ms	36.5 ms	0.7
BAC AP count	3 ± 0	3	0
Mean somatic AP ISI	9.9 ± 0.85 ms	9.4 ms	0.6
Somatic AHP depth	−65 ± 4 mV	-66 mV	0.3
Somatic AP peak	25 ± 5 mV	34 mV	1.8
Somatic AP half-width	2 ± 0.5 ms	1.6 ms	0.8
AP count (somatic current injection only)	1 ± 0	1	0
bAP amplitude at 835 µm from the soma	45 ± 10 mV	14 mV	3.1
bAP amplitude at 1015 µm from the soma	36 ± 9.33 mV	9 mV	2.9

Table S3 (related to Figure 3). Optimization targets for biophysical L5PT models. Features of membrane potential used to constrain the intrinsic physiology of the L5PT models. Empirical features were adapted from (Hay et al., 2011). ISI: inter-spike interval; AHP: after-hyperpolarization. Model features based on optimized parameters. Difference between model features and average experimental features given in units of STD of the experimental features.

Cell type	uPSP Mean (mV) (exp. / fit)	uPSP Median (mV) (exp. / fit)	uPSP Max. (mV) (exp. / fit)	Conductance per synapse (nS)
L2PY	0.49 / 0.43	0.35 / 0.37	1.90 / 2.50	1.47
L3PY	0.49 / 0.44	0.35 / 0.39	1.90 / 1.98	1.68
L4 (SP, PY)	0.35 / 0.35	0.33 / 0.30	1.00 / 1.41	1.14
L5IT	0.47 / 0.40	0.33 / 0.35	1.25 / 1.70	1.38
L5PT	0.46 / 0.43	0.36 / 0.39	1.50 / 1.46	1.59
L6(CC, INV)	0.44 / 0.42	0.31 / 0.40	1.80 / 1.26	1.63
L6CT	0.44 / 0.39	0.31 / 0.36	1.80 / 1.73	1.80
VPM	0.571 / 0.51	0.463 / 0.44	1.18 / 1.80	1.78

Table S4 (related to Figure 3). Cell type-specific synaptic strengths. Features of uPSP distributions of L5PTs for synaptic input from each presynaptic excitatory cell type, and the respectively fitted synaptic conductance values. Empirical values for uPSP amplitude distributions of synapses from IC cell types (Schnepel et al., 2015) and VPM thalamus (Constantinople and Bruno, 2013) were adapted as reported previously.